NIH Public Access
Author Manuscript
AJR Am J Roentgenol. Author manuscript; available in PMC 2013 November 28.

Published in final edited form as:
AJR Am J Roentgenol. 2013 September ; 201(3): . doi:10.2214/AJR.12.9544.

Perfusion MRI: The Five Most Frequently Asked Clinical Questions

Marco Essig[1], **Thanh Binh Nguyen**[2], **Mark S. Shiroishi**[3], **Marc Saake**[1], **James M. Provenzale**[4,5], **David S. Enterline**[4], **Nicoletta Anzalone**[6], **Arnd Dörfler**[1], **Àlex Rovira**[7], **Max Wintermark**[8], and **Meng Law**[3]

[1]Department of Neuroradiology, University of Erlangen-Nuremberg, Maximiliansplatz 1, 91054 Erlangen, Germany

[2]Department of Medical Imaging, The Ottawa Hospital, Ottawa, ON, Canada

[3]Division of Neuroradiology, Department of Radiology, Keck School of Medicine, University of Southern California, Los Angeles, CA

[4]Department of Radiology, Duke University Medical Center, Durham, NC

[5]Department of Radiology and Imaging Sciences, Oncology and Biomedical Engineering, Emory University School of Medicine, Atlanta, GA

[6]Scientific Institute H. S. Raffaele, Milan, Italy

[7]MR Unit, Department of Radiology, Universitat Autònoma de Barcelona, Hospital Vall d'Hebron, Barcelona, Spain

[8]Department of Neuroradiology, University of Virginia, Charlottesville, VA

Abstract

OBJECTIVE—This article addresses questions that radiologists frequently ask when planning, performing, processing, and interpreting MRI perfusion studies in CNS imaging.

CONCLUSION—Perfusion MRI is a promising tool in assessing stroke, brain tumors, and neurodegenerative diseases. Most of the impediments that have limited the use of perfusion MRI can be overcome to allow integration of these methods into modern neuroimaging protocols.

Keywords

CNS imaging; contrast agents; gadobutrol; perfusion MRI

Cerebral perfusion MRI is being used routinely for an increasing number of indications, including tumor imaging, cerebrovascular disease, infectious diseases, epilepsy, Alzheimer disease, and psychiatric disorders such as schizophrenia. This article addresses the most common questions about the established indications for perfusion MRI, namely tumor and stroke.

© American Roentgen Ray Society

Address correspondence to M. Essig (marco.essig@uk-erlangen.de).

NIH-PA Author Manuscript
NIH-PA Author Manuscript
NIH-PA Author Manuscript

NIH-PA Author Manuscript

NIH-PA Author Manuscript

NIH-PA Author Manuscript

Question 1: How Does One Interpret Perfusion MR Images of Patients With Brain Tumors?

The ability of conventional MRI to provide detailed anatomic images has greatly benefited the detection of CNS tumors. Characterizing the grade and malignant potential of a tumor with conventional MRI, however, has been less successful, in particular because factors such as T1 and T2 relaxation times (related to tumor angiogenesis and the integrity of the blood-brain barrier of neoplastic tissue) are only moderately specific indicators of malignancy [1, 2]. Perfusion MRI techniques, by contrast, can be used for quantitative assessment of specific pathophysiologic parameters, more accurate grading of intracranial tumors, and differentiation of tumors from normal tissue.

A corollary to question 1 is, How does one evaluate the perfusion data in cerebral neoplastic lesions and quantify the results? Perfusion MRI data can be analyzed with many methods, but there is no standardization of technique [3, 4]. However, some general recommendations can be made. The method chosen depends on whether one is focused on a routine clinical question versus a clinical research question, in which more semi-quantitative and quantitative approaches are needed. For routine clinical practice, simple visual inspection of the parametric color maps may be sufficient to detect normal versus abnormal regions. Although this type of analysis is not a quantitative assessment of perfusion metrics, it can be very useful in the clinical setting [5].

If semiquantitative data are desired, most often user-defined regions of interest (ROIs) can be placed in the tissue of interest and in the contralateral normal-appearing region (either white matter or gray matter) for semiquantitative analysis of signal intensity depending on the location of the lesion [6]. Although placement of multiple ROIs is the most common method of analysis, this method has an unavoidable component of subjectivity. For that reason alternative methods, such as histogram analysis, have been examined. The results appear to show that these methods can yield meaningful perfusion metrics [7, 8]. Histograms depict the heterogeneity of the ROI; however, there is loss of spatial specificity. Parametric response mapping is an advanced method of analysis. Parametric maps are coregistered over serial examinations and compared voxel by voxel before and after treatment [9]. Preliminary results appear to show promise for this technique; however, the technical demands of coregistration of image voxels can be challenging [10].

Calculation of a summary statistic such as relative cerebral blood volume (rCBV) normalized to an internal control such as normal-appearing white matter does not require determination of the arterial input function and simplifies postprocessing. Wetzel et al. [11] found that placing a minimum of four small ROIs in the areas thought to contain the highest rCBV values based on color maps and recording the maximal rCBV ($rCBV_{max}$) had the greatest intraobserver and interobserver reproducibility. Visual inspection of the signal intensity–time curves resulting from ROI placement can be performed for qualitative interpretation. If the area under the curve increases, the curve can be considered consistent with tumor, whereas a decrease can be considered consistent with radiation necrosis or a nonneoplastic lesion. For absolute quantification of dynamic susceptibility contrast (DSC) perfusion MRI–derived cerebral blood flow (CBF) and CBV, deconvolution of the concentration of tissue tracer by the arterial input function is required. This remains a great technical challenge, however, and is the focus of intense research efforts [12, 13].

Similarly, visual inspection and semiquantitative analysis of signal intensity–time curves in dynamic contrast-enhanced (DCE) perfusion MRI from user-defined ROIs have been used to differentiate benign from malignant breast lesions [14]. Although these methods have shortcomings, such as possible influence from scanner settings or patient physiologic

NIH-PA Author Manuscript

NIH-PA Author Manuscript

NIH-PA Author Manuscript

characteristics not related to the tumor, decreased physiologic specificity, and difficulty in comparing results obtained at different times and institutions, these methods do have potential as more practical, user-friendly alternatives to more complicated multicompartmental pharmacokinetic methods. Some reports have shown the potential of these methods for differentiating progressive glioblastoma from treatment-induced and delayed radiation necrosis in brain tumors [15–17].

Question 2: What Is the Added Value of Perfusion MRI of Brain Tumors?

Considerable clinical experience has been gained with perfusion MRI of cerebral tumors. Perfusion MRI with DSC and DCE techniques can play an important role at the major clinical decision points: diagnosis, intervention, and posttreatment monitoring.

Dynamic Susceptibility Contrast Perfusion MRI

Relative CBV values derived from perfusion DSC-MRI studies correlate with findings at conventional angiographic evaluation of tumor vascular density, PET findings, and histologic measures of tumor neovascularity [18, 19] (Fig. 1). Cerebral tumors present with increased blood volume and flow compared with the surrounding normal white matter as a result of tumor-induced angiogenesis. Radiotherapy reduces the intratumoral blood volume. High intratumoral rCBV values are associated with a worse outcome after radiotherapy, indicating that profuse tumor-induced angiogenesis correlates with more aggressive tumor growth [20]. Additional capabilities of perfusion MRI may include noninvasive assessment of delayed radiation injury, which is characterized by fibrinoid necrosis, endothelial thickening, hyalinization, and occlusion of small vessels [15, 21].

Relative CBV is markedly decreased in normal-appearing brain tissue after whole-brain radiotherapy, a phenomenon that contrasts to the relatively moderate decrease in rCBV of normal tissue in patients with grade 2 astrocytoma after conformal radiotherapy [20–22]. Advanced radiotherapeutic techniques result in measurable sparing of normal tissues with regard to blood volume. Perfusion imaging studies of patients with brain metastases show that measurement of relative CBF (rCBF) and rCBV before radiation therapy may be used to predict response [20, 23]. After radiosurgery, rCBV decreases in patients with tumor remission and stable disease despite a temporary enlargement of tumor volume, which contrasts to the increase in rCBV found in patients with tumor progression after 3 months of follow-up [20].

DSC-MRI–derived metrics other than rCBV have been proposed for different brain tumor assessments. Percentage signal intensity recovery is a less complex alternative measure of microvascular permeability and can be derived from the DSC-MRI signal intensity–time curve [24, 25]. Peak height is another alternative metric that can be derived from the DSC-MRI signal intensity–time curve that has been highly correlated with rCBV [26].

Glioma Grading and Outcome

It is well known that there is a strong correlation between glioma grade and rCBV from perfusion DSC-MRI [18, 27–29] (Fig. 2). The transfer constant (K^{trans}) also appears to be correlated with glioma grade; however, the correlation of rCBV and grade appear stronger [30]. Values and thresholds vary in the literature, likely stemming from differences in image acquisition, postprocessing, and interpretation (Table 1).

Bisdas et al. [31] found that $rCBV_{max}$ greater than 4.2 was predictive of recurrence and that $rCBV_{max}$ of 3.8 or less was predictive of 1-year survival of astrocytoma, excluding tumors with oligodendroglial components. These values are higher than those previously reported by Lev et al. [32] (1.5) and Law et al. [33] (1.75), possibly because of differences in imaging

NIH-PA Author Manuscript

NIH-PA Author Manuscript

NIH-PA Author Manuscript

techniques, tumor types, and methods. Law et al. found that an rCBV threshold of 1.75 was predictive of median time to progression independently of histopathologic result. Patients with high initial relative rCBV appeared to have more rapid progression than those with a low rCBV. Relative CBV has also been found to increase up to 12 months before contrast enhancement is visualized at conventional MRI of low-grade gliomas undergoing malignant transformation [34].

Biopsy Guidance

Biopsy of brain tumors is guided by either contrast-enhanced CT or MRI [35]. Sampling error is a major pitfall with this method because the most malignant portion of the tumor may not necessarily show contrast enhancement. It has been estimated that 38% of anaplastic astrocytomas are not substantially enhancing and that as many as 25% of brain tumors are likely undergraded as a result [32]. Other limitations to histopathologic grading include a lack of consensus regarding multiple approaches in grading systems and relatively low reproducibility of interpretation [36]. Relative CBV maps can be used to better select the highest-grade regions for biopsy targets of both enhancing and nonenhancing tumors [6] (Fig. 2).

Primary Glioma Versus Solitary Metastatic Brain Tumor

The conventional imaging appearances of a primary glioma and a solitary brain metastatic tumor can be quite similar, and it can be difficult to differentiate them. Examination of the rCBV in the peritumoral region surrounding a mass may improve differentiation of these lesions. The rCBV surrounding a high-grade glioma appears to be greater than that of a solitary metastatic tumor [6, 37] (Fig. 3). Peak height and percentage signal intensity recovery from perfusion DSC-MRI also appear useful for discriminating the two lesions [25, 38]. The peak height of the peritumoral region in glioblastoma appears elevated compared with a solitary metastatic lesion. The percentage signal intensity recovery of the peritumoral region and contrast-enhancing region of a meta-static lesions also is lower (increased permeability) than in a glioblastoma. These findings are consistent with the respective histopathologic features. The peritumoral region of a metastatic tumor is composed of pure vasogenic edema without infiltrative tumor. The peritumoral region of a high-grade glioma, however, is composed of both vasogenic edema and infiltrative tumor, which can extend far beyond the T2-hyperintense margins of the peritumoral region [39, 40]. The differences in permeability can be explained by the finding that the capillaries of a glioblastoma retain a defective blood-brain barrier, whereas the microvasculature of metastatic lesions resembles the normal capillaries of the tissue of origin without a blood-brain barrier [41]. Results with other perfusion techniques, such as arterial spin labeling (ASL), have shown that CBF is significantly elevated in the peritumoral region of glioblastomas compared with meta-static lesions [42] (Table 1).

Primary Glioma Versus Lymphoma

Primary cerebral lymphoma can appear similar to high-grade glioma and other high-grade tumors at conventional contrast-enhanced MRI [6] (Fig. 4). Because of a lack of the striking angiogenesis usually seen in high-grade glioma, lymphomas have lower rCBV than high-grade gliomas [43] (Fig. 4. and Table 1).

Meningiomas, Tumefactive Demyelinating Lesions, and Infection

Although, in general, meningiomas are benign, they can have much higher rCBV than intraaxial tumors (Fig. 5). This is likely due to their marked vascularity and the complete absence of a blood-brain barrier in these tumors, which can produce erroneously high or low rCBV values [6]. DSC-MRI has been used to characterize the blood supply of meningiomas

NIH-PA Author Manuscript

NIH-PA Author Manuscript

NIH-PA Author Manuscript

[44]. The typical blood supply of a benign meningioma is derived from dural branches of the external carotid artery. These vessels do not have a blood-brain barrier, and therefore the signal intensity–time curves show little or no return of signal intensity to baseline after the first pass of gadolinium-based contrast agent. Parasitization of pial arteries occurs as the meningioma enlarges. These arteries do have a blood-brain barrier and therefore exhibit greater return of the baseline signal intensity after the first pass. Meningiomas, which have more pial-cortical blood supply, tend to be more aggressive and recur at higher rates [44].

Martin et al. [45] used selective intraarterial injection of a gadolinium-based contrast agent into meningiomas to evaluate the perfusion characteristics and blood supply of these tumors before and after embolization in a combined angiography-MRI suite. The territories of the meningioma fed by the selected arteries and the treated and untreated regions of the tumor were visualized. Relative CBV and relative mean time to enhancement were found to be significantly elevated in the peritumoral edema of malignant compared with benign meningiomas, but there was no significant difference in tumoral parenchymal values [46]. The greater rCBV in malignant tumors was attributed to angiogenesis and tumor invasion of the adjacent brain tissue [47]. The greater relative mean time to enhancement was thought to result from the multifactorial effect of tumor size, microvascular permeability, vessel tortuosity, and vascular compression [48, 49]. Another study [49] showed that atypical meningiomas had elevated rCBV and K^{trans} compared with benign meningiomas, although only the K^{trans} difference was statistically significant (Table 2).

Tumefactive demyelinating lesions are defined as single or multiple focal brain lesions that may be clinically and radiographically indistinguishable from tumors, presenting a diagnostic challenge. These lesions commonly exhibit, in the acute stage of development, peripheral contrast enhancement, perilesional edema, and mass effect, mimicking the typical imaging features of high-grade glioma (glioblastoma multiforme) [50]. Although the presence of some imaging findings (Baló-like pattern, open-ring enhancement) suggest a diagnosis of tumefactive demyelinating lesions [51], which can be made with a high degree of certainty, not infrequently definitive diagnosis requires biopsy despite clinical suspicion of demyelination [52].

Perfusion DSC-MRI has been used to discriminate active tumefactive demyelinating lesions from high-grade gliomas and, compared with MR spectroscopy, can be better implemented in the routine diagnostic work-up of brain mass lesions of unknown origin because it can be easily performed immediately before acquisition of contrast-enhanced images with minimal increase in examination time. Some studies have shown that DSC-MRI can be used to differentiate grade 4 gliomas from active tumefactive demyelinating lesions on the basis of results of analysis of rCBV [53]. This difference can be explained by important biologic dissimilarities between these two types of lesions. Grade 4 glioma is characterized by the presence of neoangiogenesis and vascular endothelial proliferation, which leads to substantial increases in rCBV. Tumefactive demyelinating lesions, however, are characterized by intrinsically normal or inflamed vessels with only mild inflammatory angiogenesis [54], producing a normal or mildly increased rCBV (Fig. 6). It has been found that rCBV values in acute tumefactive demyelinating lesions cannot be used to differentiate active tumefactive demyelinating lesions from grade 2 and 3 gliomas [55], because both types of lesion have a similar rCBV increase. However, active tumefactive demyelinating lesions usually present an MRI diagnostic challenge in grade 4 but not grade 2 and 3 gliomas.

Differentiation of Recurrent Tumor and Delayed Radiation Necrosis

Differentiating recurrent tumor and delayed radiation necrosis is critical because they have vastly different management strategies. Patients with recurrent tumor may undergo further

NIH-PA Author Manuscript

NIH-PA Author Manuscript

NIH-PA Author Manuscript

surgery and chemotherapy and radiation therapy whereas those with delayed radiation necrosis may be treated conservatively with steroids. Conventional contrast-enhanced MRI is not reliable for differentiating delayed radiation necrosis from recurrent tumor because both can appear as a contrast-enhancing mass with surrounding edema [56]. Relative CBV appears to be elevated in patients with recurrent tumor compared with rCBV in patients with delayed radiation necrosis, likely reflective of the increased vascular proliferation and leaky capillaries of recurrent tumor, whereas delayed radiation necrosis is composed of extensive fibrinoid necrosis, vascular dilatation, and endothelial injury [24, 57–59]. Barajas et al. [24] reported increased peak height and rCBV and lower relative percentage signal intensity recovery in recurrent glioblastoma than in delayed radiation necrosis. Experience with DCE-MRI in the context of delayed radiation necrosis is limited but also seems to indicate that delayed radiation necrosis has lower permeability than recurrent tumor [15] (Fig. 7). Results of a study that included 18 patients with high-grade glioma appeared to support this finding. A K^{trans} threshold greater than 0.19 had 100% sensitivity and 83% specificity in the detection of recurrent glioma versus delayed radiation necrosis [60] (Table 3).

Dynamic Contrast-Enhanced Perfusion MRI

Perfusion DCE-MRI technique and pharmacokinetic analysis are more complex than perfusion DSC-MRI, and this is likely a major reason perfusion DCE-MRI has not gained wider popularity. Semiquantitative DCE techniques not based on pharmacokinetic models exist, including evaluation of signal intensity–time curves (so-called curveology). Although semi-quantitative metrics are less physiologically specific, they are relatively simple to derive and interpret. These techniques have been useful in tumors outside the brain, such as cancer of the prostate, cervix, and breast [14, 17, 61–63]. Using analysis of signal intensity–time curves, Narang et al. [16] found that the normalized maximum slope of enhancement in the initial vascular phase could be used to discriminate recurrent tumor from treatment-induced necrosis.

Posttherapeutic Evaluation of Glioblastoma

Changes in the 2D area of contrast enhancement, known as the Macdonald criteria, are the most commonly used method for evaluating the therapeutic response of high-grade gliomas [64]. However, reliance on contrast enhancement is problematic because it is a nonspecific finding that reflects breakdown of the blood-brain barrier. Contrast-enhancing lesions found after therapy could be due to tumor, but other processes, such as radiation necrosis, postsurgical changes, postictal changes, and changes in steroid dosage, may be responsible [56, 65, 66]. In the glioblastoma literature, both pseudoprogression and pseudoresponse are major concerns that have gained attention. In pseudoprogression, a transient increase in contrast enhancement is noted in the first 3–6 months after completion of radiation therapy as part of the standard regimen of chemoradiation with temozolomide [67, 68]. The use of conventional contrast-enhanced MRI is not adequate for differentiating pseudoprogression and true early progression, and to our knowledge no other imaging technique has been validated to differentiate the two entities [69, 70]. Data appear to show that rCBV is significantly elevated in true early progression compared with pseudo-progression [71, 72]. Because of concerns regarding the effect of contrast leakage on the accuracy of rCBV, the use of a blood-pool agent, such as ferumoxytol, instead of a gadolinium-based contrast agent may improve differentiation of pseudoprogression from true early progression [73] (Table 4).

Little is known about the use of DCE-MRI in the evaluation of pseudoprogression. According to results extrapolated from the limited experience with delayed radiation necrosis, it is likely that permeability is lower in pseudoprogression when compared with a gadolinium-based contrast agent [15, 24, 74].

NIH-PA Author Manuscript

NIH-PA Author Manuscript

NIH-PA Author Manuscript

Another situation in which reliance on conventional contrast-enhanced MRI can be problematic is the use of antiangiogenic agents such as bevacizumab in the care of patients with recurrent glioblastoma. These agents are associated with high response rates and 6-month progression-free survival, but their effects on overall survival appear modest [75]. The term "pseudoresponse" refers to the rapid decrease in contrast enhancement without significant tumor reduction after treatment with antiangiogenic agents [76]. This phenomenon has been attributed to a decrease in vascular permeability due to normalization of the blood-brain barrier induced by these agents [77]. This vascular normalization has also been found to be reversible in patients who need a drug holiday [75]. A vascular normalization index composed of changes in K^{trans}, rCBV, and circulating type IV collagen appeared to correlate with progression-free and overall survival as early as 1 day after treatment with cediranib [78]. Perfusion DCE-MRI can also be used for preoperative tumor grading [79].

Evidence of Clinical Benefit

Many studies have documented the utility of perfusion DCE-MRI in predicting tumor grade and prognosis and in differentiating tumor recurrence from radiation necrosis [18, 24, 28, 32, 58, 80] (Fig. 8). However, despite its existence for more than 20 years, perfusion MRI remains essentially a research tool and not the standard of care for the evaluation of brain tumors. There are several reasons for this: First, no specific reimbursement for perfusion MRI exists; second, no gadolinium-based contrast agent has been approved specifically for brain perfusion MRI; and perhaps most important, there is a paucity of high-quality data showing actual clinical importance in the care of neurooncology patients.

A single-center prospective study including patients with glioma addressed this issue [81]. In that study, 59 consecutively registered patients with glioma were evaluated by three neuroradiologists in consensus. Conventional MRI sequences were followed by qualitative analysis of perfusion images (which included both DSC and ASL perfusion MRI techniques). These imaging data were evaluated in conjunction with clinical data and were assessed in a multidisciplinary manner with a clinical neurooncology team. Hypothetical treatment plans were developed for each patient prospectively, first with conventional MRI and then with conventional MRI combined with perfusion MRI. The overall conclusion was that the addition of perfusion imaging appeared to have a significant effect on neuroradiologists' and clinicians' confidence in assessment of tumor status and the course of clinical management. Larger multicenter confirmatory studies are needed.

Question 3: How Do I Interpret Perfusion MRI for Patients With Stroke?

The usual sequences used in acute stroke MRI include perfusion-weighted imaging, diffusion-weighted imaging (DWI), T2-weighted FLAIR imaging, T2*-weighted gradient-echo imaging with susceptibility weighted imaging, and MR angiography [82] (Fig. 9). DWI is the most sensitive method of detecting hyperacute ischemia [83, 84]. However, normalization of diffusion restriction can occur during the early phase of ischemia, so the initial diffusion abnormality may not exactly correspond to the infarct core [85]. Perfusion DSC-MRI can be used to estimate the extent and location of the hypoperfused brain parenchyma. Maps of CBF, CBV, mean transit time (MTT), and time to peak are typically generated in perfusion DSC-MRI (Fig. 9). Time to peak of impulse response is also often used and represents the time to peak of the residue function. Because of the technical difficulty of quantitative imaging, relative values of perfusion metrics are often used rather than quantitative values [86, 87], but this substitution is thought to introduce large errors. MTT and time to peak impulse response are the perfusion metrics often used in clinical practice, though there is currently no widely accepted standardized method of perfusion imaging analysis in acute stroke [88, 89].

NIH-PA Author Manuscript

NIH-PA Author Manuscript

NIH-PA Author Manuscript

Question 4: What Is the Added Value of Perfusion MRI in the Evaluation of Stroke?

Perfusion DSC-MRI is used in combination with DWI in the evaluation of patients presenting with acute stroke and transient ischemic attacks and in the evaluation of the ischemic penumbra. The presence of an ischemic penumbra defines the amount of brain tissue at risk of infarction that can be potentially salvaged with early reperfusion (Fig. 10). In two clinical trials—Diffusion and Perfusion Imaging Evaluation for Understanding Stroke Evolution (DEFUSE) and Echoplanar Imaging Thrombolytic Evaluation Trial (EPITHET)—more than one half of patients presenting with an acute stroke 3–6 hours after onset had an ischemic penumbra, which was defined as a perfusion volume abnormality at least 20% and 10 mL greater than the diffusion volume abnormality. The results of these two trials showed that a perfusion-diffusion mismatch could be used to select patients for IV tissue plasminogen activator (tPA) treatment beyond the 3-hour window.

Although the ischemic penumbra has been widely accepted as a target for therapy, there is no consensus on the absolute thresholds for defining the ischemic penumbra for two reasons. First, DSC-MRI shows only rCBF with current acquisition and postprocessing techniques used in clinical practice. Second, many perfusion parameters (CBV, CBF, MTT, time to peak, time to peak impulse response) can be used, and their values may change depending on the postprocessing technique.

Despite the limitations, it is agreed that the infarct core is best evaluated with DWI. Areas of restricted diffusion from cytotoxic edema usually represent the irreversibly infarcted tissue but may include some penumbral tissue in rare situations in which patients undergo early recanalization with intraarterial therapy [90]. The penumbra is determined from the perfusion abnormality present on a time-domain parameter map such as the time to peak, MTT, or time to peak impulse response, which reflects the delay of the bolus agent reaching the ischemic area. A time to peak impulse response longer than 6 seconds and penumbra–to–core lesion volume ratio greater than 1.2 were used in clinical trials for selecting patients who would benefit from thrombectomy more than 3 hours after stroke onset.

In patients with an unknown time of onset of stroke, perfusion-weighted imaging may be used to select those still in the therapeutic window. A time to peak longer than 3 seconds without diffusion changes has been found accurate for differentiating penumbra from hyperacute stroke (0–6 hours) versus acute stroke (7–12 hours) [91]. In the Extending the Time for Thrombolysis in Emergency Neurological Deficits (EXTEND) trial, the efficacy of IV tissue plasminogen activator in the treatment of patients with wake-up stroke is being tested with penumbral mismatch as an inclusion criterion [92].

CBV, CBF, and MTT—the three main parameters of perfusion—are each useful for imaging acute cerebral ischemia. CBV maps correlate best with the final infarct volume, implying that rCBV maps incorporate flow via collateral vessels to provide a snapshot of cerebrovascular reserve. The gray-white differences in CBF and CBV maps can be difficult to interpret. By contrast, MTT is an easy-to-interpret parameter that shows homogeneity in normal areas. MTT maps tend toward a binary classification, that is, showing either normal or uniformly abnormal areas with no gradation, which can be helpful for identifying areas of abnormal hemodynamics [20]. Infarct size, however, tends to be overestimated on MTT maps.

MTT and other timing maps appear to be inadequate for differentiating levels of hemodynamic compromise. The explanation is that the feature that makes the maps easy to interpret—that is, normal versus abnormal—does not allow gradation of abnormalities. In

NIH-PA Author Manuscript

NIH-PA Author Manuscript

NIH-PA Author Manuscript

addition, it does not seem possible to differentiate acute from chronic hemodynamic compromise with any MRI or non-MRI perfusion technique. Adding DWI to the protocol allows this distinction. Study results have also indicated that perfusion MRI may yield useful information about nonacute cerebrovascular disease, including stenosis and occlusion of arteries supplying the brain, and about venous disease.

Identification of the tissue at risk of infarction, or ischemic penumbra, is important for deciding which patients may benefit from risky therapies [93]. It was initially thought that the diffusion-weighted abnormality corresponded to the infarct core, whereas the perfusion abnormality was reflective of the hypoperfused tissue [94]. The ischemic penumbra was thought to represent the volumetric difference between the diffusion and perfusion abnormalities, commonly referred to as the diffusion-perfusion mismatch [95]. However, more recent data have led to a reconsideration of this concept, because not all diffusion abnormalities necessarily result in infarction. The possibility also exists that the perfusion abnormality may represent areas of benign oligemia [85, 90]. The existence of multiple postprocessing methods can result in variability in the use of thresholds to establish ischemic penumbra and infarct core [88].

As the time between stroke onset and treatment increases, the clinical benefit from thrombolysis decreases. Diffusion-perfusion mismatch imaging has been used in multiple clinical trials focused on patient selection for thrombolytic therapy beyond the 3-hour window of stroke onset. Examples are the Desmoteplase in Acute Ischemic Stroke (DIAS), Dose Escalation of Desmoteplase for Acute Stroke (DEDAS), DIAS 2, DEFUSE, and EPITHET trials [96–99]. In general, the results of these trials appeared to support the use of mismatch imaging to select patients who would benefit from thrombolytic therapy. The exception was the DIAS 2 study, which incorporated CT perfusion imaging, which did not appear to show clinical benefit of desmoteplase treatment compared with placebo. The inclusion of mild strokes with their high response rate might have contributed to the lack of apparent benefit in the treatment group [99]. A meta-analysis of these trials concluded that although it appears that delayed thrombolysis (beyond 3 hours after stroke onset) based on mismatch imaging is associated with increased reperfusion-recanalization and possibly clinical benefit, there appears to be high risk of intracerebral hemorrhage and possibly increased mortality [100]. The lack of technical standardization of penumbral imaging remains a major challenge. Further phase 3 multicenter trials are needed for validation of mismatch imaging biomarkers and establishment of accurate threshold values [82, 88, 89, 101].

Question 5: What Specific Protocols Can Be Used for Cerebral Perfusion MRI?

Integration of perfusion techniques into a modern neuroimaging protocol is not complex but has a few prerequisites and entails use of contrast media and injection techniques. Typical protocols for tumor and stroke imaging are summarized in Appendixes 1 and 2. The requirements for the MRI system are not highly specific. However, because ASL perfusion and DSC perfusion are based on echo-planar techniques, the MRI unit should allow these fast acquisition techniques. For fast acquisition in contrast-enhanced perfusion MRI and MR angiography, automated contrast injection is preferred.

A double injection of contrast medium has been proposed for both brain tumor and stroke protocols [89, 102]. For tumor imaging, a combination of DCE and DSC perfusion and for stroke a combination of MR angiography and DSC perfusion are suggested. With the use of modern techniques, such as imaging with high-relaxivity and high-concentration contrast media in combination with high-end MRI equipment, one can split a single dose of contrast

NIH-PA Author Manuscript

NIH-PA Author Manuscript

NIH-PA Author Manuscript

medium into two injections [102]. With older technology or conventional contrast media, this might not be sufficient, leading to injection of a higher contrast dose. In general, it is preferred that DSC acquisition be performed with the second injection, because this allows a preload of contrast medium in brain tumors, and the preload of contrast medium does not influence the MR angiographic results in stroke.

An alternative perfusion sequence that has gained great interest, especially for indications that would not require contrast injections, is ASL. In this method, labeled blood is used as an endogenous tracer for quantification of CBF. The method works best with high-field MRI systems with a higher signal-to-noise ratio and longer sampling period because of the longer relaxation times. ASL has been used in several studies of brain tumors, including initial workup and follow-up management [20, 34, 42, 81]. It can also be easily integrated into protocols, but the method is more time-consuming than perfusion DSC-MRI and more sensitive to patient motion and susceptibility artifacts, as from intratumoral bleeding. ASL may serve as an alternative for imaging of patients with impaired renal function.

ASL can also be used for imaging of patients with acute stroke. Because of its high sensitivity to minor perfusion deficits, ASL can be used both in major stroke and in transient ischemia. A major limitation of the use of ASL in acute stroke assessment is that the patients often cannot cooperate, and the temporal resolution is substantially inferior than that of contrast enhancement [82]. With an optimized technique and fast acquisition, ASL may also be applied in acute stroke [103].

For patients who can cooperate and who have nonacute disorders, ASL has proved effective for assessment of impaired blood flow even with non-high-end equipment. In one study [104], ASL performed as well as perfusion DSC-MRI in the evaluation of patients with transient ischemic events. Another report [105] describes a potential role in the assessment of cerebrovascular reactivity in patients with clinically significant stenoocclusive disease and in follow-up after stroke. The results of these studies suggest that ASL can be of value in the care of patients with transient ischemia, especially if use of contrast media is contraindicated.

Summary and Outlook

Perfusion MRI with either DCE or DSC technique has become well established for the assessment of stroke and cerebral tumors. For these techniques to gain broader acceptance, however, challenges must be overcome, including lack of standardization in acquisition and postprocessing. Additional indications in which perfusion MRI would be beneficial include neurodegenerative and psychiatric diseases such as Alzheimer disease, schizophrenia, depression, and infectious CNS diseases [106–111].

Most experience has been gained in the assessment of Alzheimer disease, the most common neurodegenerative disease. Perfusion and metabolism in Alzheimer disease have traditionally been measured with SPECT and PET [107]. Perfusion MRI, however, has emerged as a functional imaging technique in the care of these patients because it is more accessible, has higher spatial resolution, and is more economically efficient than nuclear medicine techniques. Both perfusion DSC-MRI and ASL perfusion MRI have been used. Because of its completely noninvasive nature, ASL perfusion MRI has been particularly attractive. Decreased CBF is seen not only throughout the course of Alzheimer disease but also during mild cognitive impairment (preclinical phase) and in persons with normal cognitive function who are at increased risk of Alzheimer disease (genetic factors or family history) [112, 113]. Global and regional hypoperfusion, particularly in the posterior cingulate and precuneus and lateral parietal cortex, is evident in Alzheimer disease.

NIH-PA Author Manuscript

NIH-PA Author Manuscript

NIH-PA Author Manuscript

Acknowledgments

M. Essig, T. B. Nguyen, and M. S. Shiroishi contributed equally to this article.

M. Essig serves on scientific advisory boards for Bayer HealthCare and Medical Imaging Heidelberg, has received speaker honoraria from Bayer HealthCare and Bracco, and has received research support from Bayer HealthCare.

T. B. Nguyen has received grant support from the Brain Tumour Foundation of Canada and is a paid consultant for Bayer HealthCare.

M. S. Shiroishi serves as a consultant for Bayer HealthCare.

J. M. Provenzale has received research funding from GE Healthcare; is a Scientific Advisory Board member for Bayer HealthCare; is a consultant for Millennium Pharmaceuticals, Amgen, and Biomedical Systems; is on the Data Safety Management Board of Theradex, Inc.; and is an author for and stockholder in Amirsys, Inc.

N. Anzalone has received speaker honoraria and serves as a consultant for Bayer HealthCare.

À. Rovira serves on scientific advisory boards for NeuroTEC, Bayer HealthCare, and BTG International Ltd; has received speaker honoraria from Bayer HealthCare, Stendhal America, Sanofi-Aventis, Bracco, Merck-Serono, Teva Pharmaceutical Industries Ltd, and Biogen Idec; has received research support from Bayer HealthCare; and serves as a consultant for Novartis.

M. Wintermark has received grants from Philips Healthcare and GE Healthcare.

M. Law serves on scientific advisory boards for Bayer HealthCare and Toshiba Medical Systems; has received speaker honoraria from Siemens Healthcare, iCAD Inc, Bayer HealthCare, Bracco, and Prism Clinical Imaging; and has received research support from the NIH and Bayer HealthCare.

Supported in part by a GE Healthcare/RSNA Research Scholar Grant, Zumberge Research Grant, and Southern California Clinical and Translational Science Institute (CTSI) Pilot Grant (NIH CTSA grant 5 UL1 RR031986-02) (M. S. Shiroishi).

References

1. Law M, Meltzer DE, Cha S. Spectroscopic magnetic resonance imaging of a tumefactive demyelinating lesion. Neuroradiology. 2002; 44:986–989. [PubMed: 12483443]
2. Schaefer PW, Grant PE, Gonzalez RG. Diffusion-weighted MR imaging of the brain. Radiology. 2000; 217:331–345. [PubMed: 11058626]
3. Shiroishi MS, Lacerda S, Law M. Perfusion MRI of brain neoplasms. Curr Med Imaging Rev. 2010; 6:232–245.
4. Shiroishi MS, Habibi M, Rajderkar D, et al. Perfusion and permeability MR imaging of gliomas. Technol Cancer Res Treat. 2011; 10:59–71. [PubMed: 21214289]
5. Wintermark M, Sesay M, Barbier E, et al. Comparative overview of brain perfusion imaging techniques. Stroke. 2005; 36:e83–e99. [PubMed: 16100027]
6. Cha S, Knopp EA, Johnson G, Wetzel SG, Litt AW, Zagzag D. Intracranial mass lesions: dynamic contrast-enhanced susceptibility-weighted echo-planar perfusion MR imaging. Radiology. 2002; 223:11–29. [PubMed: 11930044]
7. Law M, Young R, Babb J, Pollack E, Johnson G. Histogram analysis versus region of interest analysis of dynamic susceptibility contrast perfusion MR imaging data in the grading of cerebral gliomas. AJNR. 2007; 28:761–766. [PubMed: 17416835]
8. Young R, Babb J, Law M, Pollack E, Johnson G. Comparison of region-of-interest analysis with three different histogram analysis methods in the determination of perfusion metrics in patients with brain gliomas. J Magn Reson Imaging. 2007; 26:1053–1063. [PubMed: 17896374]
9. Tsien C, Galban CJ, Chenevert TL, et al. Parametric response map as an imaging biomarker to distinguish progression from pseudoprogression in high-grade glioma. J Clin Oncol. 2010; 28:2293–2299. [PubMed: 20368564]
10. Gerstner ER, Sorensen AG. Diffusion and diffusion tensor imaging in brain cancer. Semin Radiat Oncol. 2011; 21:141–146. [PubMed: 21356481]

NIH-PA Author Manuscript

NIH-PA Author Manuscript

NIH-PA Author Manuscript

11. Wetzel SG, Cha S, Johnson G, et al. Relative cerebral blood volume measurements in intracranial mass lesions: interobserver and intraobserver reproducibility study. Radiology. 2002; 224:797–803. [PubMed: 12202717]
12. Bleeker EJ, van Buchem MA, van Osch MJ. Optimal location for arterial input function measurements near the middle cerebral artery in first-pass perfusion MRI. J Cereb Blood Flow Metab. 2009; 29:840–852. [PubMed: 19142193]
13. Østergaard L. Principles of cerebral perfusion imaging by bolus tracking. J Magn Reson Imaging. 2005; 22:710–717. [PubMed: 16261573]
14. Rieber A, Brambs HJ, Gabelmann A, Heilmann V, Kreienberg R, Kühn T. Breast MRI for monitoring response of primary breast cancer to neo-adjuvant chemotherapy. Eur Radiol. 2002; 12:1711–1719. [PubMed: 12111062]
15. Lacerda S, Law M. Magnetic resonance perfusion and permeability imaging in brain tumors. Neuroimaging Clin N Am. 2009; 19:527–557. [PubMed: 19959004]
16. Narang J, Jain R, Arbab AS, et al. Differentiating treatment-induced necrosis from recurrent/progressive brain tumor using nonmodel-based semiquantitative indices derived from dynamic contrast-enhanced T1-weighted MR perfusion. Neuro Oncol. 2011; 13:1037–1046. [PubMed: 21803763]
17. Yankeelov TE, Gore JC. Dynamic contrast enhanced magnetic resonance imaging in oncology: theory, data acquisition, analysis, and examples. Curr Med Imaging Rev. 2009; 3:91–107. [PubMed: 19829742]
18. Knopp EA, Cha S, Johnson G, et al. Glial neoplasms: dynamic contrast-enhanced T2*-weighted MR imaging. Radiology. 1999; 211:791–798. [PubMed: 10352608]
19. Sugahara T, Korogi Y, Kochi M, et al. Correlation of MR imaging-determined cerebral blood volume maps with histologic and angiographic determination of vascularity of gliomas. AJR. 1998; 171:1479–1486. [PubMed: 9843274]
20. Essig M, Giesel F, Le-Huu M, Stieltjes B, von Tengg H, Weber MA. Perfusion MRI in CNS disease: current concepts. Neuroradiology. 2004; 46(suppl 2):s201–s207. [PubMed: 15645153]
21. Fatterpekar GM, Galheigo D, Narayana A, Johnson G, Knopp E. Treatment-related change versus tumor recurrence in high-grade gliomas: a diagnostic conundrum—use of dynamic susceptibility contrast-enhanced (DSC) perfusion MRI. AJR. 2012; 198:19–26. [PubMed: 22194475]
22. Matsusue E, Fink JR, Rockhill JK, Ogawa T, Maravilla KR. Distinction between glioma progression and post-radiation change by combined physiologic MR imaging. Neuroradiology. 2010; 52:297–306. [PubMed: 19834699]
23. Essig M, Waschkies M, Wenz F, Debus J, Hentrich HR, Knopp MV. Assessment of brain metastases with dynamic susceptibility-weighted contrast-enhanced MR imaging: initial results. Radiology. 2003; 228:193–199. [PubMed: 12832582]
24. Barajas RF Jr, Chang JS, Segal MR, et al. Differentiation of recurrent glioblastoma multiforme from radiation necrosis after external beam radiation therapy with dynamic susceptibility-weighted contrast-enhanced perfusion MR imaging. Radiology. 2009; 253:486–496. [PubMed: 19789240]
25. Cha S, Lupo JM, Chen MH, et al. Differentiation of glioblastoma multiforme and single brain metastasis by peak height and percentage of signal intensity recovery derived from dynamic susceptibility-weighted contrast-enhanced perfusion MR imaging. AJNR. 2007; 28:1078–1084. [PubMed: 17569962]
26. Lupo JM, Cha S, Chang SM, Nelson SJ. Dynamic susceptibility-weighted perfusion imaging of high-grade gliomas: characterization of spatial heterogeneity. AJNR. 2005; 26:1446–1454. [PubMed: 15956514]
27. Aronen HJ, Gazit IE, Louis DN, et al. Cerebral blood volume maps of gliomas: comparison with tumor grade and histologic findings. Radiology. 1994; 191:41–51. [PubMed: 8134596]
28. Law M, Yang S, Wang H, et al. Glioma grading: sensitivity, specificity, and predictive values of perfusion MR imaging and proton MR spectroscopic imaging compared with conventional MR imaging. AJNR. 2003; 24:1989–1998. [PubMed: 14625221]
29. Shin JH, Lee HK, Kwun BD, et al. Using relative cerebral blood flow and volume to evaluate the histopathologic grade of cerebral gliomas: preliminary results. AJR. 2002; 179:783–789. [PubMed: 12185064]

NIH-PA Author Manuscript

NIH-PA Author Manuscript

NIH-PA Author Manuscript

30. Law M, Yang S, Babb JS, et al. Comparison of cerebral blood volume and vascular permeability from dynamic susceptibility contrast-enhanced perfusion MR imaging with glioma grade. AJNR. 2004; 25:746–755. [PubMed: 15140713]
31. Bisdas S, Kirkpatrick M, Giglio P, Welsh C, Spampinato MV, Rumboldt Z. Cerebral blood volume measurements by perfusion-weighted MR imaging in gliomas: ready for prime time in predicting short-term outcome and recurrent disease? AJNR. 2009; 30:681–688. [PubMed: 19179427]
32. Lev MH, Rosen BR. Clinical applications of intracranial perfusion MR imaging. Neuroimaging Clin N Am. 1999; 9:309–331. [PubMed: 10318717]
33. Law M, Young RJ, Babb JS, et al. Gliomas: predicting time to progression or survival with cerebral blood volume measurements at dynamic susceptibility-weighted contrast-enhanced perfusion MR imaging. Radiology. 2008; 247:490–498. [PubMed: 18349315]
34. Danchaivijitr N, Waldman AD, Tozer DJ, et al. Low-grade gliomas: do changes in rCBV measurements at longitudinal perfusion-weighted MR imaging predict malignant transformation? Radiology. 2008; 247:170–178. [PubMed: 18372467]
35. Kelly PJ, Daumas-Duport C, Kispert DB, Kall BA, Scheithauer BW, Illig JJ. Imaging-based stereotaxic serial biopsies in untreated intracranial glial neoplasms. J Neurosurg. 1987; 66:865–874. [PubMed: 3033172]
36. Coons SW, Johnson PC, Scheithauer BW, Yates AJ, Pearl DK. Improving diagnostic accuracy and interobserver concordance in the classification and grading of primary gliomas. Cancer. 1997; 79:1381–1393. [PubMed: 9083161]
37. Law M, Cha S, Knopp EA, Johnson G, Arnett J, Litt AW. High-grade gliomas and solitary metastases: differentiation by using perfusion and proton spectroscopic MR imaging. Radiology. 2002; 222:715–721. [PubMed: 11867790]
38. Cha S, Lu S, Johnson G, Knopp EA. Dynamic susceptibility contrast MR imaging: correlation of signal intensity changes with cerebral blood volume measurements. J Magn Reson Imaging. 2000; 11:114–119. [PubMed: 10713942]
39. Strugar J, Rothbart D, Harrington W, Criscuolo GR. Vascular permeability factor in brain metastases: correlation with vasogenic brain edema and tumor angiogenesis. J Neurosurg. 1994; 81:560–566. [PubMed: 7523634]
40. Strugar JG, Criscuolo GR, Rothbart D, Harrington WN. Vascular endothelial growth/permeability factor expression in human glioma specimens: correlation with vasogenic brain edema and tumor-associated cysts. J Neurosurg. 1995; 83:682–689. [PubMed: 7674019]
41. Rojiani AM, Dorovini-Zis K. Glomeruloid vascular structures in glioblastoma multiforme: an immunohistochemical and ultrastructural study. J Neurosurg. 1996; 85:1078–1084. [PubMed: 8929498]
42. Weber MA, Zoubaa S, Schlieter M, et al. Diagnostic performance of spectroscopic and perfusion MRI for distinction of brain tumors. Neurology. 2006; 66:1899–1906. [PubMed: 16801657]
43. Calli C, Kitis O, Yunten N, Yurtseven T, Islekel S, Akalin T. Perfusion and diffusion MR imaging in enhancing malignant cerebral tumors. Eur J Radiol. 2006; 58:394–403. [PubMed: 16527438]
44. Saloner D, Uzelac A, Hetts S, Martin A, Dillon W. Modern meningioma imaging techniques. J Neurooncol. 2010; 99:333–340. [PubMed: 20809250]
45. Martin AJ, Cha S, Higashida RT, et al. Assessment of vasculature of meningiomas and the effects of embolization with intra-arterial MR perfusion imaging: a feasibility study. AJNR. 2007; 28:1771–1777. [PubMed: 17885240]
46. Zhang H, Rodiger LA, Shen T, Miao J, Oudkerk M. Perfusion MR imaging for differentiation of benign and malignant meningiomas. Neuroradiology. 2008; 50:525–530. [PubMed: 18379768]
47. Arai M, Kashihara K, Kaizaki Y. Enhancing gliotic cyst wall with microvascular proliferation adjacent to a meningioma. J Clin Neurosci. 2006; 13:136–139. [PubMed: 16410217]
48. Cha S, Yang L, Johnson G, et al. Comparison of microvascular permeability measurements, K(trans), determined with conventional steady-state T1-weighted and first-pass T2*-weighted MR imaging methods in gliomas and meningiomas. AJNR. 2006; 27:409–417. [PubMed: 16484420]
49. Yang S, Law M, Zagzag D, et al. Dynamic contrast-enhanced perfusion MR imaging measurements of endothelial permeability: differentiation between atypical and typical meningiomas. AJNR. 2003; 24:1554–1559. [PubMed: 13679270]

NIH-PA Author Manuscript

NIH-PA Author Manuscript

NIH-PA Author Manuscript

50. Lucchinetti CF, Gavrilova RH, Metz I, et al. Clinical and radiographic spectrum of pathologically confirmed tumefactive multiple sclerosis. Brain. 2008; 131:1759–1775. [PubMed: 18535080]
51. Malhotra HS, Jain KK, Agarwal A, et al. Characterization of tumefactive demyelinating lesions using MR imaging and in-vivo proton MR spectroscopy. Mult Scler. 2009; 15:193–203. [PubMed: 19181773]
52. Kurihara N, Takahashi S, Furuta A, et al. MR imaging of multiple sclerosis simulating brain tumor. Clin Imaging. 1996; 20:171–177. [PubMed: 8877168]
53. Hourani R, Brant LJ, Rizk T, Weingart JD, Barker PB, Horska A. Can proton MR spectroscopic and perfusion imaging differentiate between neoplastic and nonneoplastic brain lesions in adults? AJNR. 2008; 29:366–372. [PubMed: 18055564]
54. Kirk J, Plumb J, Mirakhur M, McQuaid S. Tight junctional abnormality in multiple sclerosis white matter affects all calibres of vessel and is associated with blood-brain barrier leakage and active demyelination. J Pathol. 2003; 201:319–327. [PubMed: 14517850]
55. Blasel S, Pfeilschifter W, Jansen V, Mueller K, Zanella F, Hattingen E. Metabolism and regional cerebral blood volume in autoimmune inflammatory demyelinating lesions mimicking malignant gliomas. J Neurol. 2011; 258:113–122. [PubMed: 20803026]
56. Kumar AJ, Leeds NE, Fuller GN, et al. Malignant gliomas: MR imaging spectrum of radiation therapy- and chemotherapy-induced necrosis of the brain after treatment. Radiology. 2000; 217:377–384. [PubMed: 11058631]
57. Barajas RF, Chang JS, Sneed PK, Segal MR, Mc-Dermott MW, Cha S. Distinguishing recurrent intra-axial metastatic tumor from radiation necrosis following gamma knife radiosurgery using dynamic susceptibility-weighted contrast-enhanced perfusion MR imaging. AJNR. 2009; 30:367–372. [PubMed: 19022867]
58. Hu LS, Baxter LC, Smith KA, et al. Relative cerebral blood volume values to differentiate high-grade glioma recurrence from posttreatment radiation effect: direct correlation between image-guided tissue histopathology and localized dynamic susceptibility-weighted contrast-enhanced perfusion MR imaging measurements. AJNR. 2009; 30:552–558. [PubMed: 19056837]
59. Oh BC, Pagnini PG, Wang MY, et al. Stereotactic radiosurgery: adjacent tissue injury and response after high-dose single fraction radiation. Part 1. Histology, imaging, and molecular events. Neurosurgery. 2007; 60:31–44. [PubMed: 17228251]
60. Bisdas S, Naegele T, Ritz R, et al. Distinguishing recurrent high-grade gliomas from radiation injury: a pilot study using dynamic contrast-enhanced MR imaging. Acad Radiol. 2011; 18:575–583. [PubMed: 21419671]
61. Alonzi R, Padhani AR, Allen C. Dynamic contrast enhanced MRI in prostate cancer. Eur J Radiol. 2007; 63:335–350. [PubMed: 17689907]
62. Mussurakis S, Gibbs P, Horsman A. Primary breast abnormalities: selective pixel sampling on dynamic gadolinium-enhanced MR images. Radiology. 1998; 206:465–473. [PubMed: 9457201]
63. Zelhof B, Lowry M, Rodrigues G, Kraus S, Turn-bull L. Description of magnetic resonance imaging-derived enhancement variables in pathologically confirmed prostate cancer and normal peripheral zone regions. BJU Int. 2009; 104:621–627. [PubMed: 19281464]
64. Macdonald DR, Cascino TL, Schold SC Jr, Cairncross JG. Response criteria for phase II studies of supratentorial malignant glioma. J Clin Oncol. 1990; 8:1277–1280. [PubMed: 2358840]
65. Clarke JL, Chang S. Pseudoprogression and pseudoresponse: challenges in brain tumor imaging. Curr Neurol Neurosci Rep. 2009; 9:241–246. [PubMed: 19348713]
66. Finn MA, Blumenthal DT, Salzman KL, Jensen RL. Transient postictal MRI changes in patients with brain tumors may mimic disease progression. Surg Neurol. 2007; 67:246–250. [PubMed: 17320628]
67. Brandes AA, Franceschi E, Tosoni A, et al. MGMT promoter methylation status can predict the incidence and outcome of pseudoprogression after concomitant radiochemotherapy in newly diagnosed glioblastoma patients. J Clin Oncol. 2008; 26:2192–2197. [PubMed: 18445844]
68. Brandsma D, Stalpers L, Taal W, Sminia P, van den Bent MJ. Clinical features, mechanisms, and management of pseudoprogression in malignant gliomas. Lancet Oncol. 2008; 9:453–461. [PubMed: 18452856]

NIH-PA Author Manuscript

NIH-PA Author Manuscript

NIH-PA Author Manuscript

69. Chaskis C, Neyns B, Michotte A, De Ridder M, Everaert H. Pseudoprogression after radiotherapy with concurrent temozolomide for high-grade glioma: clinical observations and working recommendations. Surg Neurol. 2009; 72:423–428. [PubMed: 19150114]
70. Young RJ, Gupta A, Shah AD, et al. Potential utility of conventional MRI signs in diagnosing pseudoprogression in glioblastoma. Neurology. 2011; 76:1918–1924. [PubMed: 21624991]
71. Kong DS, Kim ST, Kim EH, et al. Diagnostic dilemma of pseudoprogression in the treatment of newly diagnosed glioblastomas: the role of assessing relative cerebral blood flow volume and oxygen-6-methylguanine-DNA methyltransferase promoter methylation status. AJNR. 2011; 32:382–387. [PubMed: 21252041]
72. Mangla R, Singh G, Ziegelitz D, et al. Changes in relative cerebral blood volume 1 month after radiation-temozolomide therapy can help predict overall survival in patients with glioblastoma. Radiology. 2010; 256:575–584. [PubMed: 20529987]
73. Gahramanov S, Raslan AM, Muldoon LL, et al. Potential for differentiation of pseudoprogression from true tumor progression with dynamic susceptibility-weighted contrast-enhanced magnetic resonance imaging using ferumoxytol vs. gadoteridol: a pilot study. Int J Radiat Oncol Biol Phys. 2011; 79:514–523. [PubMed: 20395065]
74. Hazle JD, Jackson EF, Schomer DF, Leeds NE. Dynamic imaging of intracranial lesions using fast spin-echo imaging: differentiation of brain tumors and treatment effects. J Magn Reson Imaging. 1997; 7:1084–1093. [PubMed: 9400853]
75. Batchelor TT, Sorensen AG, di Tomaso E, et al. AZD2171, a pan-VEGF receptor tyrosine kinase inhibitor, normalizes tumor vasculature and alleviates edema in glioblastoma patients. Cancer Cell. 2007; 11:83–95. [PubMed: 17222792]
76. Brandsma D, van den Bent MJ. Pseudoprogression and pseudoresponse in the treatment of gliomas. Curr Opin Neurol. 2009; 22:633–638. [PubMed: 19770760]
77. Gerstner ER, Duda DG, di Tomaso E, et al. VEGF inhibitors in the treatment of cerebral edema in patients with brain cancer. Nat Rev Clin Oncol. 2009; 6:229–236. [PubMed: 19333229]
78. Sorensen AG, Batchelor TT, Zhang WT, et al. A “vascular normalization index” as potential mechanistic biomarker to predict survival after a single dose of cediranib in recurrent glioblastoma patients. Cancer Res. 2009; 69:5296–5300. [PubMed: 19549889]
79. Nguyen TB, Cron GO, Mercier JF, et al. Diagnostic accuracy of dynamic contrast-enhanced MR imaging using a phase-derived vascular input function in the preoperative grading of gliomas. AJNR. 2012; 33:1539–1545. [PubMed: 22442046]
80. Caseiras GB, Chheang S, Babb J, et al. Relative cerebral blood volume measurements of low-grade gliomas predict patient outcome in a multi-institution setting. Eur J Radiol. 2010; 73:215–220. [PubMed: 19201123]
81. Geer CP, Simonds J, Anvery A, et al. Does MR perfusion imaging impact management decisions for patients with brain tumors? A prospective study. AJNR. 2012; 33:556–562. [PubMed: 22116105]
82. Wintermark M, Albers GW, Alexandrov AV, et al. Acute stroke imaging research roadmap. AJNR. 2008; 29:e23–e30. [PubMed: 18477656]
83. Fiebach JB, Schellinger PD, Jansen O, et al. CT and diffusion-weighted MR imaging in randomized order: diffusion-weighted imaging results in higher accuracy and lower interrater variability in the diagnosis of hyperacute ischemic stroke. Stroke. 2002; 33:2206–2210. [PubMed: 12215588]
84. Saur D, Kucinski T, Grzyska U, et al. Sensitivity and interrater agreement of CT and diffusion-weighted MR imaging in hyperacute stroke. AJNR. 2003; 24:878–885. [PubMed: 12748088]
85. Fiehler J, Knudsen K, Kucinski T, et al. Predictors of apparent diffusion coefficient normalization in stroke patients. Stroke. 2004; 35:514–519. [PubMed: 14739409]
86. Rose SE, Janke AL, Griffin M, Finnigan S, Chalk JB. Improved prediction of final infarct volume using bolus delay-corrected perfusion-weighted MRI: implications for the ischemic penumbra. Stroke. 2004; 35:2466–2471. [PubMed: 15472086]
87. Thijs VN, Somford DM, Bammer R, Robberecht W, Moseley ME, Albers GW. Influence of arterial input function on hypoperfusion volumes measured with perfusion-weighted imaging. Stroke. 2004; 35:94–98. [PubMed: 14671249]

NIH-PA Author Manuscript

NIH-PA Author Manuscript

NIH-PA Author Manuscript

88. Kane I, Carpenter T, Chappell F, et al. Comparison of 10 different magnetic resonance perfusion imaging processing methods in acute ischemic stroke: effect on lesion size, proportion of patients with diffusion/perfusion mismatch, clinical scores, and radiologic outcomes. Stroke. 2007; 38:3158–3164. [PubMed: 17975106]

89. Leiva-Salinas C, Wintermark M, Kidwell CS. Neuroimaging of cerebral ischemia and infarction. Neurotherapeutics. 2011; 8:19–27. [PubMed: 21274682]

90. Kidwell CS, Alger JR, Saver JL. Beyond mismatch: evolving paradigms in imaging the ischemic penumbra with multimodal magnetic resonance imaging. Stroke. 2003; 34:2729–2735. [PubMed: 14576370]

91. Roldan-Valadez E, Gonzalez-Gutierrez O, Martinez-Lopez M. Diagnostic performance of PWI/DWI MRI parameters in discriminating hyperacute versus acute ischaemic stroke: finding the best thresholds. Clin Radiol. 2012; 67:250–257. [PubMed: 22018803]

92. Ma H, Parsons MW, Christensen S, et al. A multicentre, randomized, double-blinded, placebo-controlled phase III study to investigate extending the time for thrombolysis in emergency neurological deficits (EXTEND). Int J Stroke. 2012; 7:74–80. [PubMed: 22188854]

93. Schlaug G, Benfield A, Baird AE, et al. The ischemic penumbra: operationally defined by diffusion and perfusion MRI. Neurology. 1999; 53:1528–1537. [PubMed: 10534263]

94. Warach S, Dashe JF, Edelman RR. Clinical outcome in ischemic stroke predicted by early diffusion-weighted and perfusion magnetic resonance imaging: a preliminary analysis. J Cereb Blood Flow Metab. 1996; 16:53–59. [PubMed: 8530555]

95. Jansen O, Schellinger P, Fiebach J, Hacke W, Sartor K. Early recanalisation in acute ischaemic stroke saves tissue at risk defined by MRI. Lancet. 1999; 353:2036–2037. [PubMed: 10376621]

96. Albers GW, Thijs VN, Wechsler L, et al. Magnetic resonance imaging profiles predict clinical response to early reperfusion: the diffusion and perfusion imaging evaluation for understanding stroke evolution (DEFUSE) study. Ann Neurol. 2006; 60:508–517. [PubMed: 17066483]

97. Furlan AJ, Eyding D, Albers GW, et al. Dose escalation of desmoteplase for acute ischemic stroke (DEDAS): evidence of safety and efficacy 3 to 9 hours after stroke onset. Stroke. 2006; 37:1227–1231. [PubMed: 16574922]

98. Hacke W, Albers G, Al-Rawi Y, et al. The Desmoteplase in Acute Ischemic Stroke trial (DIAS): a phase II MRI-based 9-hour window acute stroke thrombolysis trial with intravenous desmoteplase. Stroke. 2005; 36:66–73. [PubMed: 15569863]

99. Hacke W, Furlan AJ, Al-Rawi Y, et al. Intravenous desmoteplase in patients with acute ischaemic stroke selected by MRI perfusion-diffusion weighted imaging or perfusion CT (DIAS-2): a prospective, randomised, double-blind, placebo-controlled study. Lancet Neurol. 2009; 8:141–150. [PubMed: 19097942]

100. Mishra NK, Albers GW, Davis SM, et al. Mismatch-based delayed thrombolysis: a meta-analysis. Stroke. 2010; 41:e25–e33. [PubMed: 19926836]

101. Provenzale JM, Wintermark M. Optimization of perfusion imaging for acute cerebral ischemia: review of recent clinical trials and recommendations for future studies. AJR. 2008; 191:1263–1270. [PubMed: 18806174]

102. Essig M, Anzalone N, Combs SE, et al. MR imaging of neoplastic central nervous system lesions: review and recommendations for current practice. AJNR. 2012; 33:803–817. [PubMed: 22016411]

103. Bokkers RP, Hernandez DA, Merino JG, et al. Whole-brain arterial spin labeling perfusion MRI in patients with acute stroke. Stroke. 2012; 43:1290–1294. [PubMed: 22426319]

104. Zaharchuk G, Olivot JM, Fischbein NJ, et al. Arterial spin labeling imaging findings in transient ischemic attack patients: comparison with diffusion- and bolus perfusion-weighted imaging. Cerebrovasc Dis. 2012; 34:221–228. [PubMed: 23006669]

105. Leoni RF, Mazzetto-Betti KC, Silva AC, et al. Assessing cerebrovascular reactivity in carotid steno-occlusive disease using MRI BOLD and ASL techniques. Radiol Res Pract. 2012; 2012:268483. [PubMed: 22919485]

106. Dai W, Lopez OL, Carmichael OT, Becker JT, Kuller LH, Gach HM. Mild cognitive impairment and Alzheimer disease: patterns of altered cerebral blood flow at MR imaging. Radiology. 2009; 250:856–866. [PubMed: 19164119]

NIH-PA Author Manuscript

NIH-PA Author Manuscript

NIH-PA Author Manuscript

107. Chen W, Song X, Beyea S, D'Arcy R, Zhang Y, Rockwood K. Advances in perfusion magnetic resonance imaging in Alzheimer's disease. Alzheimers Dement. 2011; 7:185–196. [PubMed: 21074500]

108. Théberge J. Perfusion magnetic resonance imaging in psychiatry. Top Magn Reson Imaging. 2008; 19:111–130. [PubMed: 19363433]

109. Peruzzo D, Rambaldelli G, Bertoldo A, et al. The impact of schizophrenia on frontal perfusion parameters: a DSC-MRI study. J Neural Transm. 2011; 118:563–570. [PubMed: 21203783]

110. Järnum H, Eskildsen SF, Steffensen EG, et al. Longitudinal MRI study of cortical thickness, perfusion, and metabolite levels in major depressive disorder. Acta Psychiatr Scand. 2011; 124:435–446. [PubMed: 21923809]

111. Muccio CF, Esposito G, Bartolini A, Cerase A. Cerebral abscesses and necrotic cerebral tumours: differential diagnosis by perfusion-weighted magnetic resonance imaging. Radiol Med (Torino). 2008; 113:747–757. [PubMed: 18414811]

112. Asllani I, Habeck C, Scarmeas N, Borogovac A, Brown TR, Stern Y. Multivariate and univariate analysis of continuous arterial spin labeling perfusion MRI in Alzheimer's disease. J Cereb Blood Flow Metab. 2008; 28:725–736. [PubMed: 17960142]

113. Austin BP, Nair VA, Meier TB, et al. Effects of hypoperfusion in Alzheimer's disease. J Alzheimers Dis. 2011; 26(suppl 3):123–133. [PubMed: 21971457]

114. American College of Radiology Imaging Network website. [Accessed May 1, 2013] Protocol RTOG 0825/ACRIN 6686. www.acrin.org/protocolsummarytable/protocol6686.aspx

NIH-PA Author Manuscript
NIH-PA Author Manuscript
NIH-PA Author Manuscript

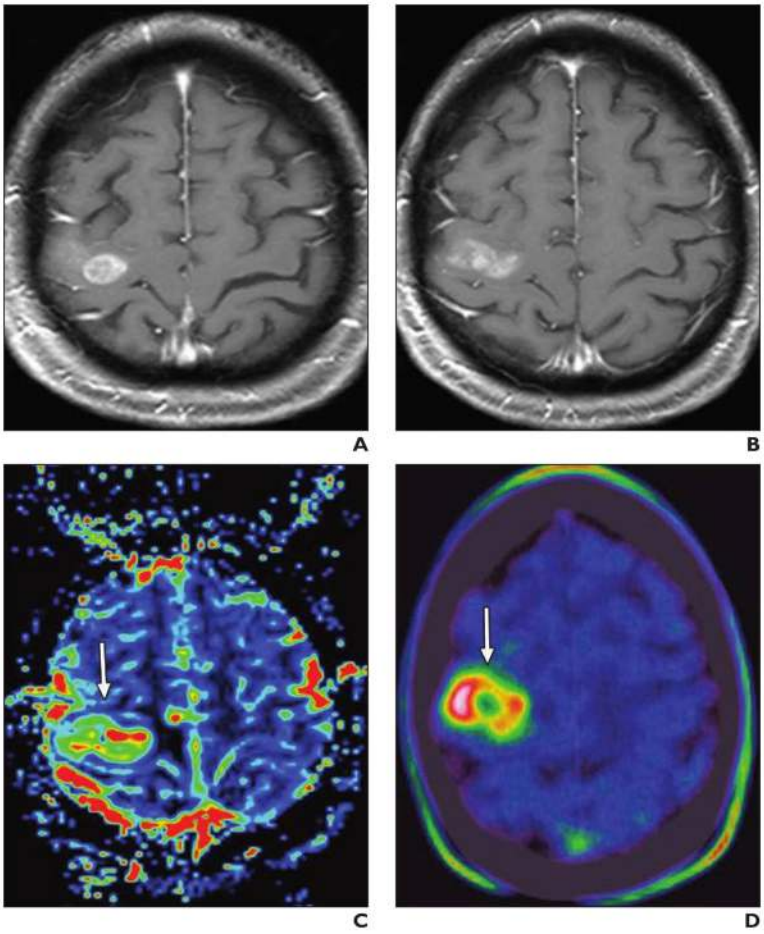

Fig. 1. Patient with histologically confirmed grade 4 astrocytoma who underwent both dynamic susceptibility contrast perfusion MRI and ^{18}F-fluorothymidine PET

A and **B,** Conventional MR images (**A** and **B,** different sections) show heterogeneous enhancing lesion with only minor mass effect.

C and **D,** Relative cerebral blood flow map (**C**) derived from dynamic susceptibility contrast perfusion MRI (0.1 mmol gadobutrol injected at 5 mL/s with 20-mL saline flush) correlates with PET findings (**D**), showing tumor (*arrow*) with high perfusion rate based on high proliferation.

NIH-PA Author Manuscript

NIH-PA Author Manuscript

NIH-PA Author Manuscript

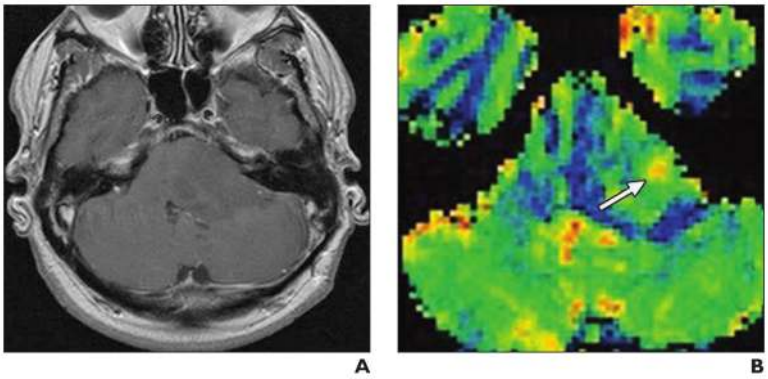

Fig. 2. 45-year-old man with suspected low-grade tumor

A, Contrast-enhanced T1-weighted spin-echo image shows no pathologic enhancement.

B, Dynamic susceptibility contrast perfusion MR image (0.1 mmol gadobutrol injected at 5 mL/s with 20-mL saline flush) shows focal hyperperfusion in center of tumor suspicious as higher-grade lesion (*arrow*). Anaplastic transformation of tumor was confirmed at targeted biopsy.

NIH-PA Author Manuscript
NIH-PA Author Manuscript
NIH-PA Author Manuscript

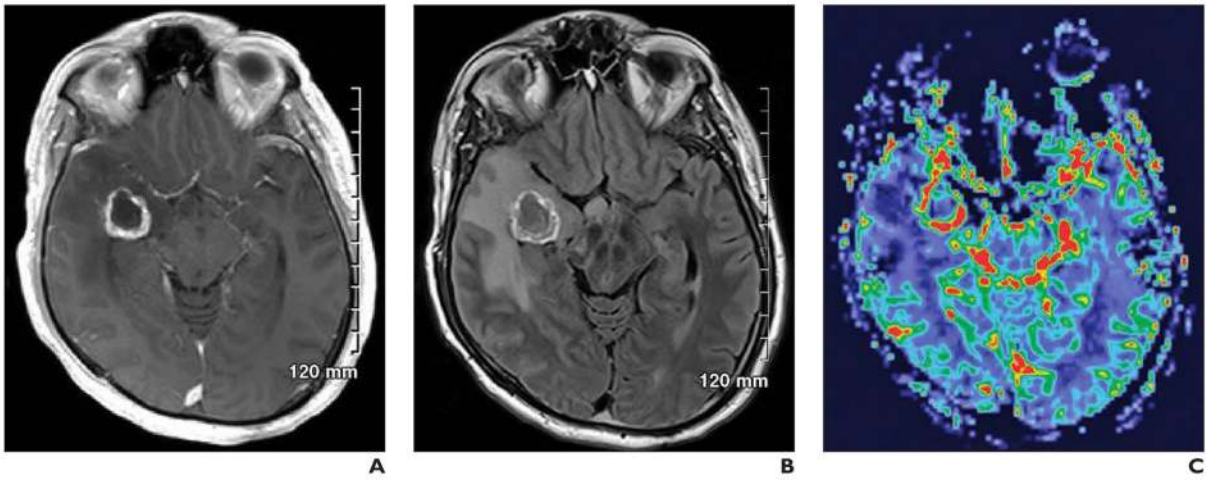

Fig. 3. 44-year-old man with history of seizures and recent foreign travel

A and **B,** Conventional MR images show multiple cerebral lesions. Differential diagnosis of right temporal lesion would include primary tumor, tuberculosis, and metastatic disease. **C,** Perfusion image (0.1 mmol of gadobutrol at 5 mL/s) shows increased relative cerebral blood flow, which suggests metastatic disease. Metastatic adenocarcinoma was found at surgery.

NIH-PA Author Manuscript
NIH-PA Author Manuscript
NIH-PA Author Manuscript

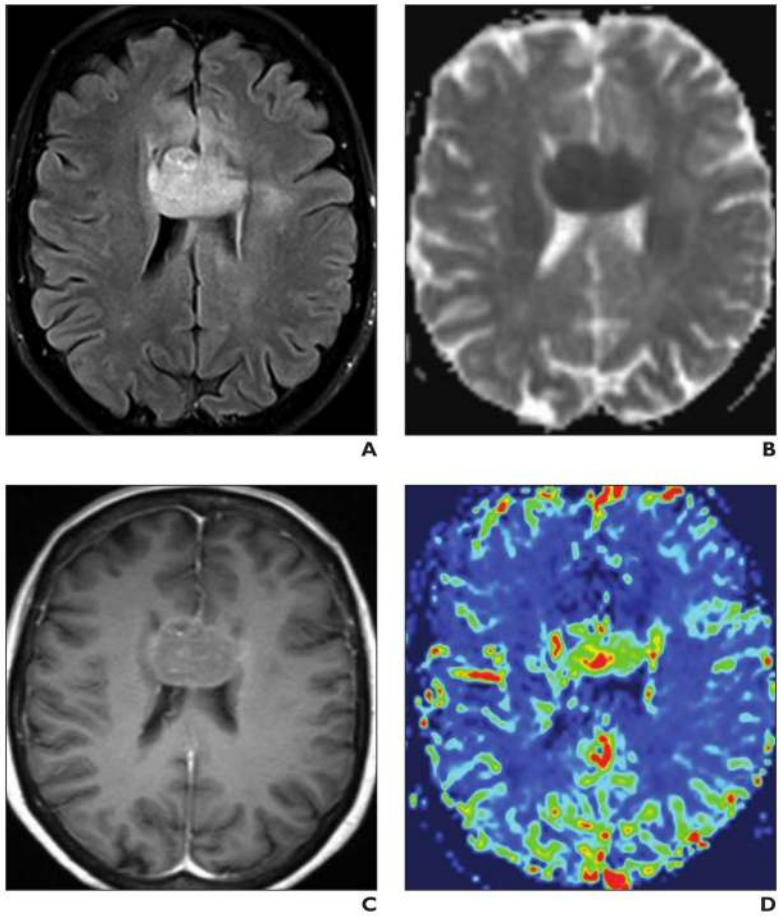

Fig. 4. 52-year-old immunocompetent man with primary corpus callosum CNS lymphoma

A–D, Brain MRI includes transverse T2-weighted FLAIR image (**A**), apparent diffusion coefficient (ADC) map (**B**), transverse contrast-enhanced T1-weighted image (**C**) (0.1 mmol of gadobutrol), and relative cerebral blood volume (rCBV) map (**D**). Homogeneous corpus callosum mass is hypointense on ADC map, consistent with restricted diffusion. Mild contrast uptake and increased signal intensity on color rCBV map indicate hyperperfusion.

NIH-PA Author Manuscript

NIH-PA Author Manuscript

NIH-PA Author Manuscript

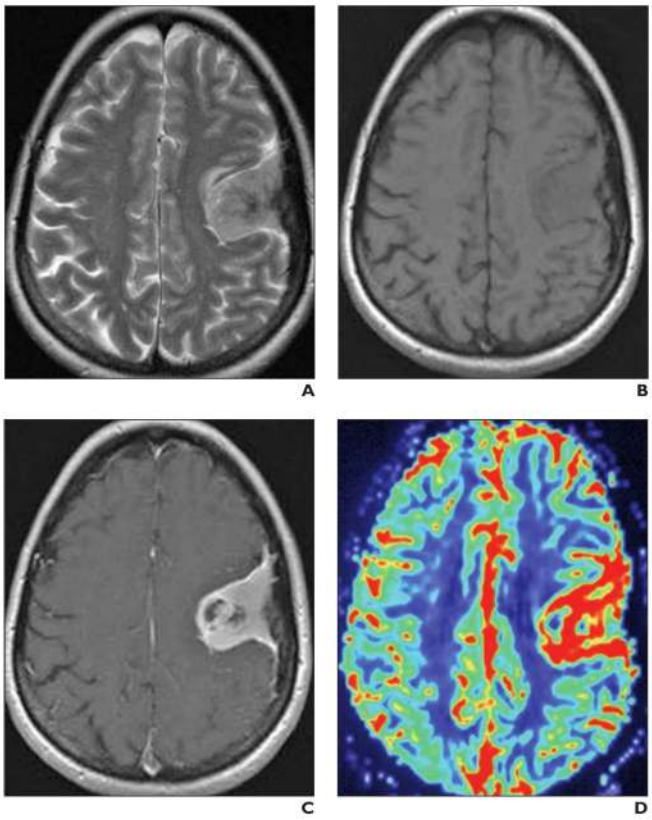

Fig. 5. 57-year-old woman with pathologically confirmed atypical meningioma (World Health Organization grade 3)

A–D, Brain MRI includes transverse T2-weighted image (**A**), transverse unenhanced (**B**) and contrast-enhanced T1-weighted (**C**) images, and transverse relative cerebral blood volume (rCBV) map (**D**) (0.1 mmol of gadobutrol at 5 mL/s). Convex enhancing left frontal mass shows small areas of necrosis and increased signal intensity on color rCBV map, indicating hyperperfusion.

NIH-PA Author Manuscript
NIH-PA Author Manuscript
NIH-PA Author Manuscript

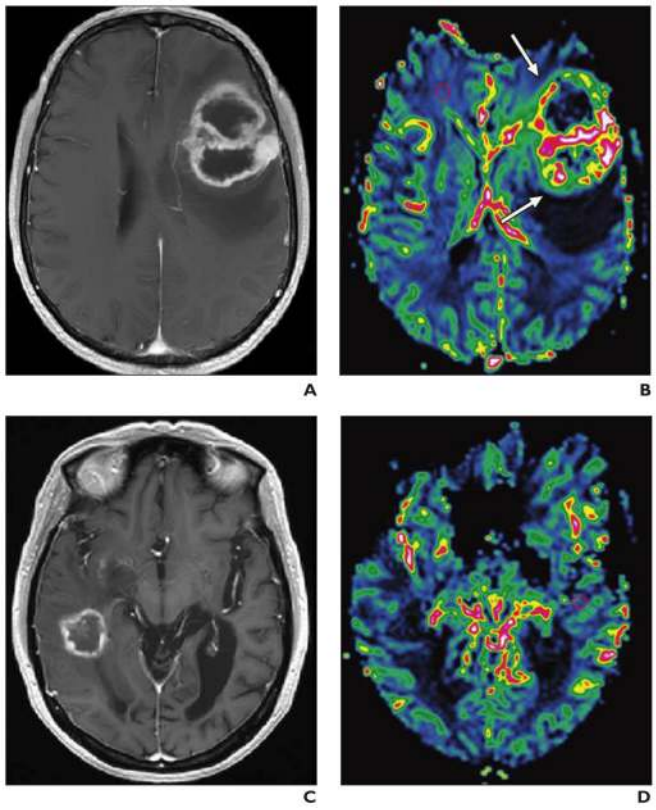

Fig. 6. Comparison of high-grade necrotic glioma and acute inflammatory-demyelinating lesion

A and **B,** 64-year-old man with high-grade necrotic glioma. Contrast-enhanced T1-weighted MR image (**A**) shows lesion pattern similar to that in **C.** Cerebral blood volume map acquired with dynamic susceptibility contrast perfusion MRI (0.1 mmol gadobutrol) (**B**), however, shows no increased perfusion.

C and **D,** 47-year-old woman with acute inflammatory-demyelinating lesion. Contrast-enhanced T1-weighted MR image (**C**) shows lesion pattern similar to that in **A.** Cerebral blood volume map acquired with dynamic susceptibility contrast perfusion MRI (0.1 mmol gadobutrol) (**D**), however, shows clear increase in cerebral blood volume (*arrows*).

NIH-PA Author Manuscript

NIH-PA Author Manuscript

NIH-PA Author Manuscript

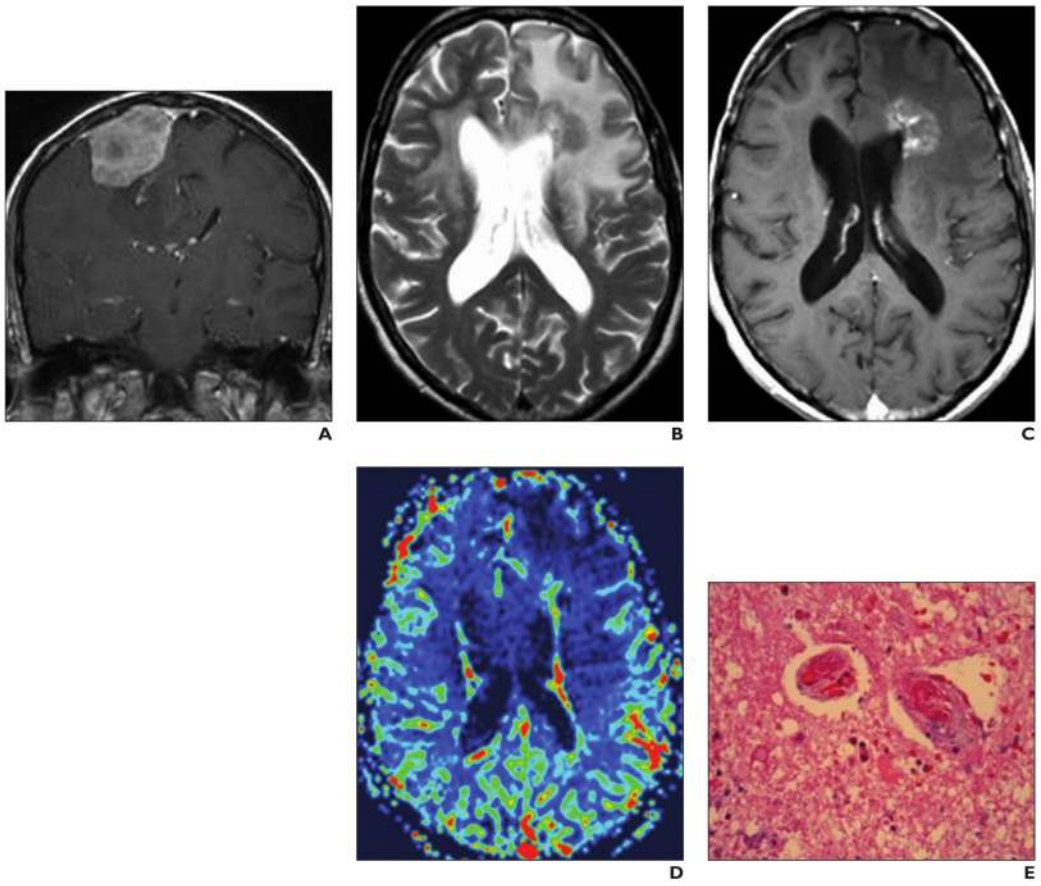

Fig. 7. 61-year-old man with left frontal lobe radiation necrosis after radiation therapy for right frontal convex malignant meningioma

A, Coronal contrast-enhanced T1-weighted MR image shows right frontal convex malignant meningioma.

B–D, Two years after radiotherapy patient had progressive headache, confusion, behavioral changes, and urinary incontinence. Transverse T2-weighted (**B**) and contrast-enhanced T1-weighted (**C**) images and relative cerebral blood volume map (**D**) (0.1 mmol/kg of gadobutrol at 5 mL/s) show diffuse radiation-induced white matter changes in both frontal lobes and deep left necrotic frontal lobe mass with irregular contrast uptake and low signal intensity in **D,** indicating hypoperfusion.

E, Photomicrograph (H and E, ×40) obtained at same time as **B–D** shows typical features of coagulation necrosis with profound vascular changes, including fibrinoid necrosis and hyalinization of wall and occlusion of lumina by fibrin thrombi.

NIH-PA Author Manuscript
NIH-PA Author Manuscript
NIH-PA Author Manuscript

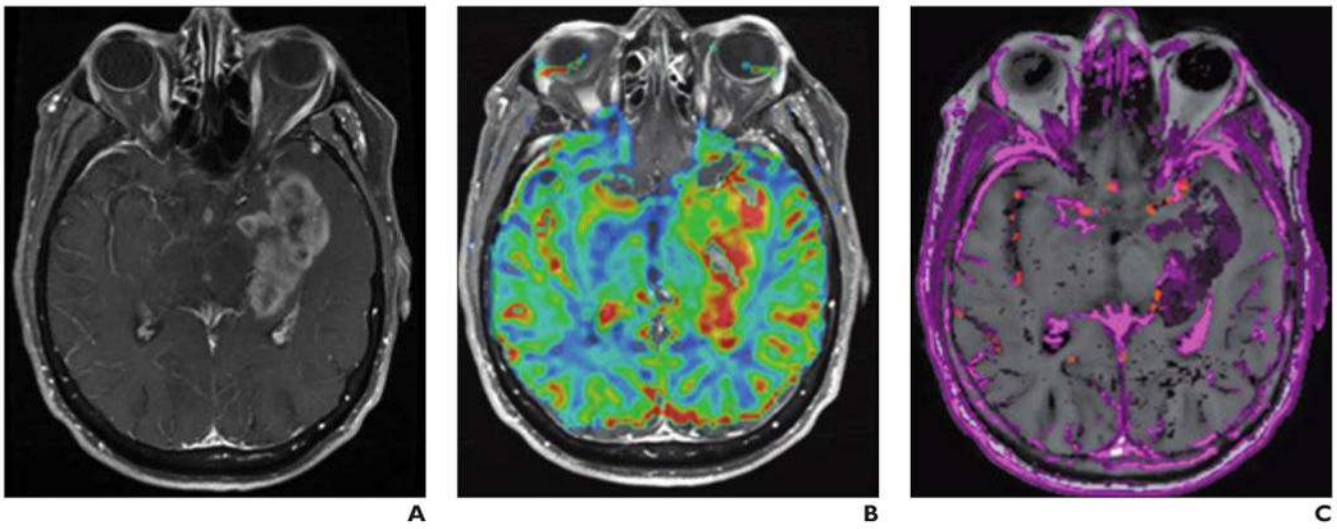

Fig. 8. 42-year-old man with left temporal lobe glioblastoma

A, Axial T1-weighted contrast-enhanced MR image shows irregular, necrotic enhancing mass in left temporal lobe.

B and **C,** Color overlays of relative cerebral blood flow (rCBV) (**B**) and K^{trans} (**C**) maps show regions of elevated rCBV and K^{trans} in tumor, confirming high tumor perfusion, proliferation, and vascularity.

NIH-PA Author Manuscript

NIH-PA Author Manuscript

NIH-PA Author Manuscript

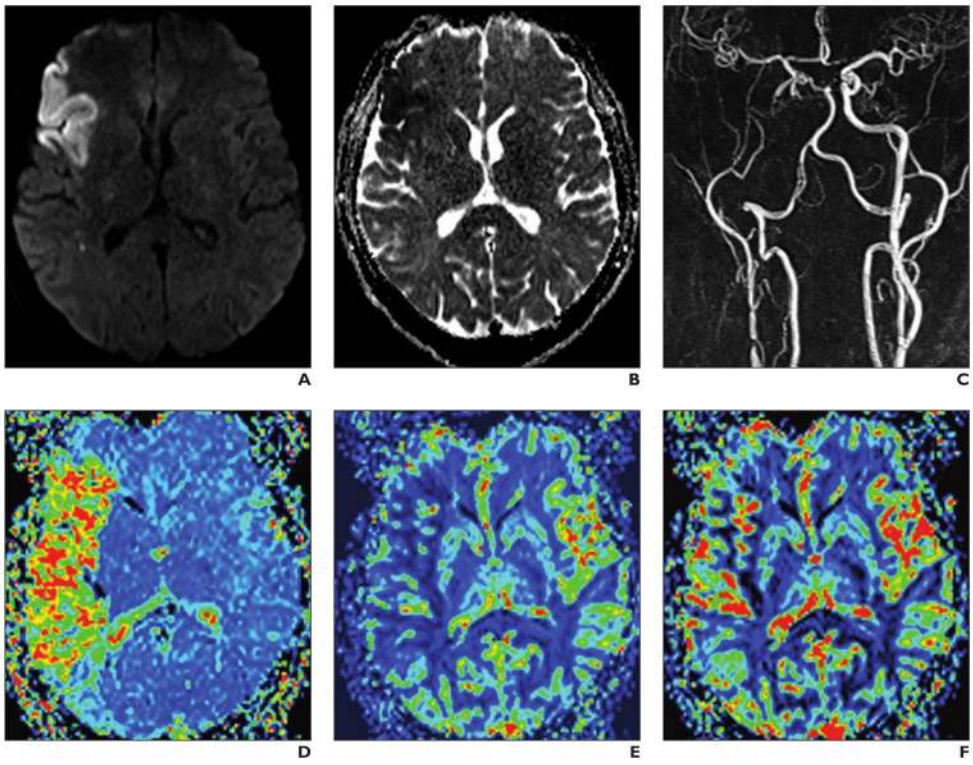

Fig. 9. 66-year-old man with right internal carotid artery occlusion, an acute middle cerebral artery infarction, and clear diffusion-perfusion mismatch

A–F, Multimodal stroke protocol consists of diffusion-weighted (**A**), ADC map (**B**), contrast-enhanced MR angiographic (MRA) (**C**), and dynamic susceptibility contrast (DSC) perfusion MR (**D–F**) images. Double-injection protocol with two times 0.05 mmol/kg gadobutrol at 3 mL/s for MRA and 5 mL/s for perfusion DSC-MRI with 20-mL saline flush each. MRA is performed before DSC imaging to avoid influences from circulating contrast media. At DSC MRI, changes are most pronounced on mean transit time (**D**) and cerebral blood flow (**E**) maps whereas cerebral blood volume map (**F**) shows minor alterations.

NIH-PA Author Manuscript
NIH-PA Author Manuscript
NIH-PA Author Manuscript

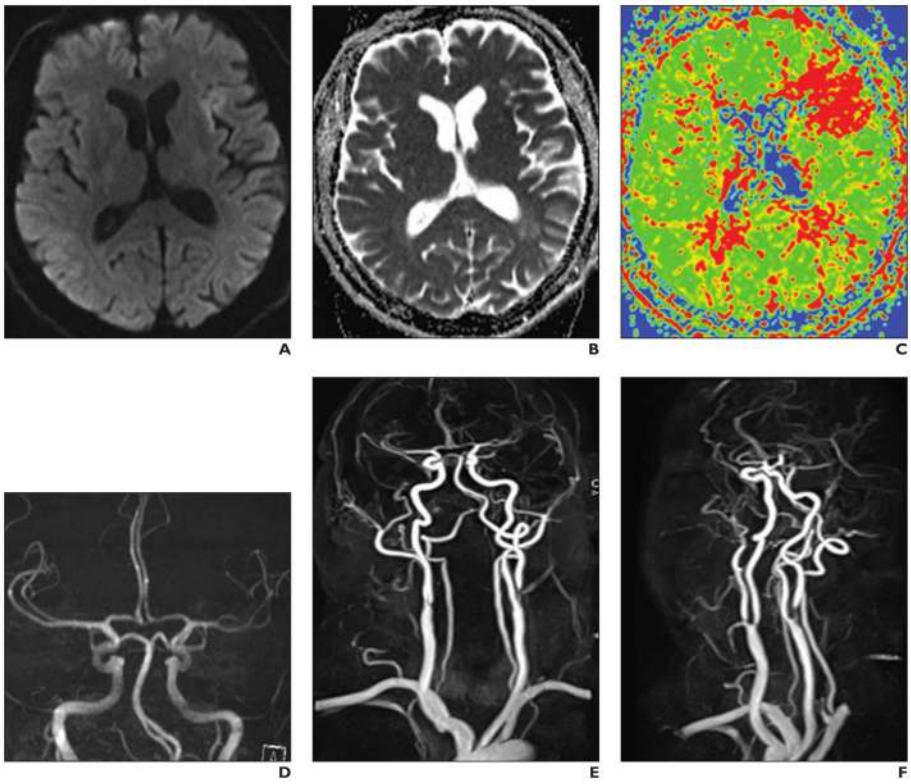

Fig. 10. 61-year-old woman with left embolic middle cerebral artery ischemia and clear diffusion-perfusion mismatch due to a symptomatic extracranial internal carotid artery stenosis

A–F, Multimodal stroke protocol with diffusion-weighted (**A**), T2-weighted (**B**), mean transit time from dynamic susceptibility contrast (DSC) perfusion MR (**C**), intracerebral time-of-flight MR angiographic (MRA) (**D**) images and contrast-enhanced MRA images of brain supplying arteries (**E** and **F,** different maximum intensity projections). Double injection protocol with two times 0.05 mmol/kg gadobutrol at 3 mL/s for MRA and 5 mL/s for perfusion with 20-mL saline flush each. MRA is performed before DSC imaging to avoid influences from circulating contrast media. In DSC imaging changes are most pronounced on mean transit time maps.

NIH-PA Author Manuscript

NIH-PA Author Manuscript

NIH-PA Author Manuscript

TABLE 1

Perfusion MRI Features Differentiating High-Grade Glioma (HGG) From Low-Grade Glioma (LGG), Solitary Metastatic Tumor, and Primary Cerebral Lymphoma

Feature	High-Grade Glioma	Comparison Tumor
Low-grade glioma		
Contrast enhancement	Common	Uncommon
Perfusion (rCBV)	Greater than in LGG	Less than in HGG
Permeability (K^{trans})	Greater than in LGG	Less than in HGG
Solitary metastatic tumor		
Contrast enhancement	Common	Common
Perfusion of peritumoral region (rCBV in relation to peak height and cerebral blood flow arterial spin labeling)	Greater than in solitary metastatic tumor	Less than in HGG
Permeability (PSR) of peritumoral region	Lower (i.e., higher PSR) than in solitary metastatic tumor	Less than in HGG
Primary cerebral lymphoma		
Perfusion (rCBV)	Greater than in lymphoma	Greater than in HGG

Note—In general, permeability and perfusion threshold values cannot be given because of differences in data acquisition and postprocessing and interpretation. Institutional techniques should be compared with particular studies described. rCBV = relative cerebral blood volume, K^{trans} = transfer constant, PSR = percentage signal recovery.

NIH-PA Author Manuscript

NIH-PA Author Manuscript

NIH-PA Author Manuscript

TABLE 2

Perfusion MRI Features Differentiating Benign and Atypical Meningioma

Feature	Benign Meningioma	Atypical Meningioma
Permeability (percentage signal recovery)	Little or no return to baseline	Greater return to baseline
Perfusion (rCBV) of peritumoral edema	Less than in atypical meningioma	Greater than in benign meningioma
Relative mean time to enhance of peritumoral edema	Less than in atypical meningioma	Greater than in benign meningioma
Permeability (K^{trans})	Less than in atypical meningioma	Greater than in benign meningioma

Note—In general, permeability and perfusion threshold values cannot be given because of differences in data acquisition and postprocessing and interpretation. Institutional techniques should be compared with particular studies described. rCBV = relative cerebral blood volume, K^{trans} = transfer constant.

NIH-PA Author Manuscript

NIH-PA Author Manuscript

NIH-PA Author Manuscript

TABLE 3

Perfusion MRI Features Differentiating Recurrent Tumor and Delayed Radiation Necrosis (DRN)

Feature	Recurrent Tumor	DRN
Contrast enhancement	Yes	Yes
Time frame	Many months to years after radiation therapy	Many months to years after radiation therapy
Perfusion (rCBV)	Significantly greater than in DRN	Significantly less than in recurrent tumor
Permeability (PSR, K^{trans})	Significantly greater than in DRN	Significantly less than in recurrent tumor

Note—In general, permeability and perfusion threshold values cannot be given because of differences in data acquisition and postprocessing and interpretation. Institutional techniques should be compared with particular studies described. rCBV = relative cerebral blood volume, PSR = percentage signal recovery, K^{trans} = transfer constant.

NIH-PA Author Manuscript

NIH-PA Author Manuscript

NIH-PA Author Manuscript

TABLE 4

Perfusion MRI Features Differentiating True Early Progression of Glioblastoma and Pseudoprogression

Feature	True Early Progression	Pseudoprogression
Contrast enhancement	Yes	Yes
Time frame	Definition varies, but typically in the first 3–6 mo after completion of radiation therapy as part of chemoradiation with temozolomide for newly diagnosed high-grade glioma	Definition varies, but typically in the first 3–6 mo after completion of radiation therapy as part of chemoradiation with temozolomide for newly diagnosed high-grade glioma
Perfusion (rCBV)	Significantly greater than in pseudoprogression	Significantly less than in true early progression

Note—It is unclear how perfusion and permeability differentiate pseudoresponse from true response. In general, permeability and perfusion threshold values cannot be given because of differences in data acquisition and postprocessing and interpretation. Institutional techniques should be compared with particular studies described. rCBV = relative cerebral blood volume.

NIH-PA Author Manuscript

NIH-PA Author Manuscript

NIH-PA Author Manuscript

APPENDIX 1

Brain Tumor Protocol

Standardized MRI Protocol In order of acquisition:

- Localizer, scout
- T1-weighted unenhanced (spin echo or gradient-recalled echo)
- T2-weighted axial (fast spin-echo)
- FLAIR (optional after contrast administration)
- Diffusion-weighted or diffusion tensor imaging (for extraction of diffusion-weighted data trace and apparent diffusion coefficient from diffusion tensor imaging)[a]
- T1-weighted map (quantitation) for dynamic contrast-enhanced MRI: 3D gradient-echo T1-weighted imaging or 2D turbo spin-echo of fast spin-echo T1-weighted imaging[a]
- T2*-weighted dynamic susceptibility contrast MRI (after presaturation dynamic contrast-enhanced sequence)[a]
- T1-weighted contrast-enhanced sequence (spin echo or gradient-recalled echo)

Optional

- Functional language, auditory, visual, motor testing, and MR spectroscopy[a]

Comments

- FLAIR can be performed before dynamic susceptibility contrast MRI
- Susceptibility-weighted imaging and gradient-recalled echo as additional optional sequences[a]

General Parameter Recommendations

- Minimum slice thickness 5 mm
- Target duration ≤30 min (maximum, 1.5–2.0 h)

Note—Protocol modified by Essig et al. [102] according to the framework of the American College of Radiology Imaging Network (ACRIN) 6686 component of the Radiation Therapy Oncology Group (RTOG) 0825 protocol [114].

[a]Part of the ACRIN 6686 protocol but can be used as an adjunct in the clinical brain tumor protocol.

NIH-PA Author Manuscript

NIH-PA Author Manuscript

NIH-PA Author Manuscript

APPENDIX 2

Stroke Imaging Protocol

Standardized MRI Protocol

- Diffusion-weighted imaging
- Gradient-recalled echo or susceptibility-weighted imaging
- T2-weighted FLAIR
- Contrast-enhanced MR angiography (first injection)
- Dynamic susceptibility contrast perfusion MRI (second injection)
- Contrast-enhanced T1-weighted sequence

General Parameter Recommendations

- Minimum slice thickness 5 mm
- Contrast-enhanced MR angiography injection: 0.05 mmol at 2 mL/s
- Dynamic susceptibility contrast perfusion MRI injection: 0.5 mmol at 5 mL/s

Alternative Protocol

- Time-of-flight MR angiography and arterial spin labeling in combination